Thermocapillary actuation by optimized resistor pattern: bubbles and droplets displacing, switching and trapping

Bertrand Selva,*[a] Vincent Miralles,[b] Isabelle Cantat*[c] and Marie-Caroline Jullien*[ab]

Received 28th January 2010, Accepted 26th March 2010
First published as an Advance Article on the web 5th May 2010
DOI: 10.1039/c001900c

We report a novel method for bubble or droplet displacement, capture and switching within a bifurcation channel for applications in digital microfluidics based on the Marangoni effect, *i.e.* the appearance of thermocapillary tangential interface stresses stemming from local surface tension variations. The specificity of the reported actuation is that heating is provided by an optimized resistor pattern (B. Selva, J. Marchalot and M.-C. Jullien, An optimized resistor pattern for temperature gradient control in microfluidics, *J. Micromech. Microeng.*, 2009, 19, 065002) leading to a constant temperature gradient along a microfluidic cavity. In this context, bubbles or droplets to be actuated entail a surface force originating from the thermal Marangoni effect. This actuator has been characterized (B. Selva, I. Cantat, and M.-C. Jullien, Migration of a bubble towards a higher surface tension under the effect of thermocapillary stress, *preprint*, 2009) and it was found that the bubble/droplet (called further element) is driven toward a high surface tension region, *i.e.* toward cold region, and the element velocity increases while decreasing the cavity thickness. Taking advantage of these properties three applications are presented: (1) element displacement, (2) element switching, detailed in a given range of working, in which elements are redirected towards a specific evacuation, (3) a system able to trap, and consequently stop on demand, the elements on an alveolus structure while the continuous phase is still flowing. The strength of this method lies in its simplicity: single layer system, *in situ* heating leading to a high level of integration, low power consumption ($P < 0.4$ W), low applied voltage (about 10 V), and finally this system is able to manipulate elements within a flow velocity up to 1 cm s^{-1}.

Introduction

In the future, one may envision microfluidic systems with mazes of microchannels along which droplets conveying solutes, materials, and particles, undergo transformations, reactions and processes.[1–3] Such systems could be used to perform all sort of bio/physico-chemical analysis or to produce novel entities. Such a prospective requires the control of elementary operations such as bubble-droplet (further called element) transport, exchanges, redirection and storage. This motivated a number of research groups to develop "digital microfluidics", a topic entirely dedicated to the handling of these elements in microsystems.

Digital microfluidics require element displacement by simple means featuring high integration rates. Within this context, the transport and handling of elements constitutes a problem.[4] To cite a few, available actuators are of electro-osmotic,[5] and dielectrophoretic[6,7] types. Mechanical actuation solutions exist as well,[8] and these necessitate implementing a double-layer technology. The application of an external pressure source is also required.

This context has rekindled interest in the Marangoni surface effect, with the objective of developing actuation systems for moving bubbles or droplets. Most of the reported papers deal with droplets in the presence of a triple line (droplet wets at least one wall). Models for the thermocapillary migration in the case of triple line have been proposed and confronted to experiments in a capillary[9,10] and over a substrate[11–13] (free surface plus triple line at the wall). Works dealing with a free surface (*i.e.* there is a wetting film between the droplet and the walls and there is consequently no more triple line) have been widely studied, *e.g.* Homsy's group,[14] at large scales (millimetre). In order to integrate Marangoni stress at the microscale at a free interface it is proposed to integrate a laser.[15,16] The authors were able to halt and redirect the displacement of a droplet. Finally, Ting *et al.*,[17] and Yap *et al.*,[18] propose the integration of heating resistors inside a microchannel which involve both Marangoni stress and modification of hydrodynamic resistance (decrease of viscosity with increasing temperature) in one daughter channel located at a T-junction. Droplet breakup in a T-junction has been widely studied and it is shown that the initial droplet extension and the capillary number (which in this case can be modified) are key parameters controlling break-up.[19]

It is necessary to distinguish the cases involving a triple line from the ones involving a free surface. Actually, in the review of Squires and Quake,[20] they clearly distinguish actuation along a triple line than an actuation along a free surface. They propose to denote the actuation along a triple line by thermowetting while thermocapillarity stands for actuation along a free surface. Our paper concerns bubbles or droplet between two plates separated by a gap of the order of 20 microns, smaller than the element diameter. The continuous phase surrounding the element wets the substrate and the element is thus separated from the substrate

[a]*SATIE, ENS-Cachan Bretagne, CNRS, UEB, av Robert Schuman, F-35170 Bruz, France. E-mail: bertrand.selva@bretagne.ens-cachan.fr*
[b]*MMN, CNRS, ESPCI Paris-Tech, 10 rue Vauquelin, F-75005 Paris, France. E-mail: caroline.jullien@espci.fr*
[c]*IPR, UMR CNRS 6251, Universite de Rennes 1, 35000 Rennes, France. E-mail: isabelle.cantat@univ-rennes1.fr*

by a thin liquid film. In that case, the physical mechanism involved in the element migration in a temperature gradient strongly differs from the case where the element is in direct contact with the substrate (no wetting film and a triple line).

This paper proposes a new method for bubble or droplet displacement and switching within a bifurcating microfluidic channel for applications in digital microfluidics, using thermo-capillary stresses induced by a constant temperature gradient. The devices proposed in this paper are operated by establishing a constant temperature gradient $\partial T/\partial x$ through the *in situ* shape optimized heating of a microfluidic cavity.[21] The interest of the presented work is that actuation allows displacing directly the elements (droplets or bubble) along an important distance; a single resistor leads to a displacement over 2.5 mm. Moreover it is shown that a single resistor design can lead to different applications (displacing, switching and trapping), thus showing the versatility of the migration method.

Principle

Actuation is obtained by the temperature gradient effect, which induces surface tension variation, expressed by the creation of a tangential interface stress on the object to be moved:

$$\vec{\tau} = \vec{\nabla}_s \cdot \partial\gamma/\partial T = \partial\gamma/\partial T \cdot \partial T/\partial x \cdot \sin\theta \cdot \vec{e}_\theta$$

where $\vec{\nabla}_s$is the surface gradient, θ the angle between $\vec{x}$ and the vector normal to the interface $\vec{e}_r$, and $\vec{e}_\theta$ the associated tangent vector (see Fig. 1a). The tangential stress leads to a liquid displacement along the interface. This kind of flow has been theoretically and experimentally described in ref. 22 leading to an analytical solution for the element velocity taking into account three independent parameters, following:

$$U = 4\,\frac{\partial\gamma}{\partial x}\,\frac{aH_0}{\alpha e\mu} \qquad (1)$$

where a is the bubble/droplet radius, e the cavity thickness, $\mu = 10^{-3}$ Pa s the dynamic viscosity, $\alpha = 0.35$ a coefficient settled by the experimental results (represented in Fig. 2), $\partial\gamma/\partial x = \partial\gamma/\partial T \cdot \partial T/\partial x$ is

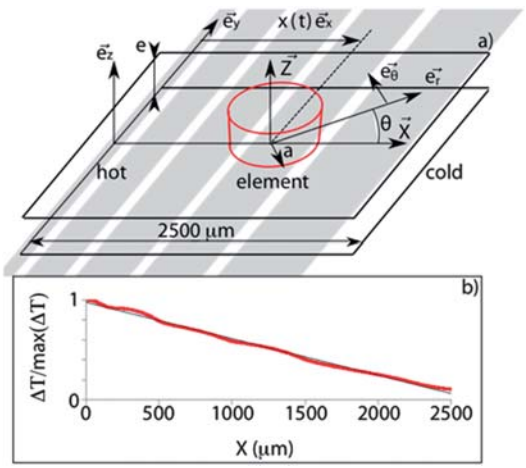

Fig. 1 (a) Sketch of the cavity and parameterization. Grey lines are the optimized resistor wires placed below the cavity. (b) Numerical temperature profile rescaled by the maximal temperature as a function of position along the cavity.

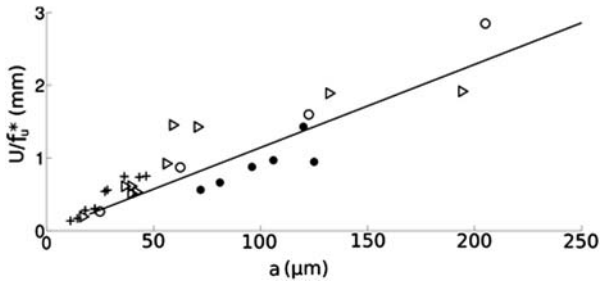

Fig. 2 Bubble velocity, for a solution of glycerol (5.8% w/w) and SDS surfactants (1.2 c.m.c. *i.e.* 0.27% w/w) and deionised water, rescaled by $f_U^* = (\partial\gamma/\partial X)(D/e\mu)$ for a cavity thickness of 22 µm and (○) $\partial\gamma/\partial X = 0.26$ Pa, (▷) $\partial\gamma/\partial X = 0.4$ Pa, (+) $\partial\gamma/\partial X = 0.79$ Pa and (●) for a cavity thickness of 37 µm and $\partial\gamma/\partial X = 1.54$ Pa. Full line represents the velocity predicted by the model.

the surface tension gradient, and H_0 the lubrication film thickness between the element and the wall cavity; H_0 is conditioned by the disjoining pressure which is imposed by the cavity thickness (*via* imposed pressure inside the bubble itself imposed by the curvature) and leads to the common film thickness, *i.e.* 17 nm (value in air).[23]

The previous equation is valid for both bubble and droplet, if (i) $a > e/2$ (*i.e.* the element has a pancake shape), (ii) the cavity thickness e is less than few hundreds of microns, (iii) the surrounding fluid wets the substrate. In this case, one remarkable feature is that the velocity is oriented toward the cold region, *i.e.* the high surface tension region, in contrast with the results obtained at the macroscale. A migration toward the high surface tension region is also obtained in the case of thermowetting between two plates, but only in the case of an element wetting the substrate (*i.e.* with a concave shape). The relation (1) also shows that decreasing cavity thickness e, increases the element velocity. This striking behaviour shows that decreasing cavity thickness favors element displacement and consequently opens the way to a high level of confinement in digital microfluidics.

The basis of the model leading to eqn (1) is the classical Hele–Shaw cell equations allowing to determine the element velocity as a function of the normal stress at the interface. This normal stress is identified and calculated at the vicinity of the wetting film using classical lubrication equations.[24]

Fig. 2 presents the experimental data, for an air bubble in a solution of deionized water, glycerol (5.8% w/w) and SDS at a concentration of 0.27% w/w equal to 1.2 times the critical micellar concentration, c.m.c. For this solution we measured $\partial\gamma/\partial T = -1.8 \times 10^{-4}$ N/m/K (see Fig. 14,[21]), in the range of working temperatures. The bubble velocity is plotted as a function of bubble radius for various imposed temperature gradients and cavity thicknesses. The straight line is the model given by eqn (1) and shows that this simple law predicts the right sign for the bubble velocity and the right scaling behaviour over the three independent parameters.

In the following, we present three applications using this physical phenomenon for microfluidic purposes: displacing, switching and capturing applications.

Root of the experimental setup

The system is composed of a cavity built in a single block of PDMS (RTV 615) and shaped by fabrication techniques conventionally used in microfluidic systems.[25] Cavity thickness

equals 22 μm. In the case of switching or capture application, the cavity is connected to a T-junction (100 μm × 200 μm), which serves to generate elements. The substrate is a glass wafer 700 μm thick over which two metal layers (150 nm for the gold connexion and 15 nm for the chromium heating wires) are deposited and the corresponding pattern is etched through S1818 photoresist. The resistor is composed of a sequence of wires placed in series and running parallel to one another.

The entire device configuration is shown in Fig. 1. It is heated by the electrical resistor, so as to obtain a constant temperature gradient along the x direction within the cavity. The width of these wires, as well as the interstices, have been optimized using a genetic algorithm, the NSGA II,[26] coupled with a finite element computation (COMSOL). The shape optimization method leading to a linear temperature profile is detailed in ref. 21 and the resulting optimized shape is sketched in Fig. 1a. The resistors are electrically insulated *via* a 20 μm thick centrifuged PDMS layer. The wafer is affixed onto an aluminium block 2 cm thick to enable guaranteeing a stationary heat balance despite the continuous application of heating power for the switching step, by playing the role of heat sink.

The temperature gradient is generated over a 2.5 mm length, which has to be compared to the one resulting from a heat flux step at the wafer surface (corresponding to the position of resistor wires). Diffusion over the step gives a temperature profile (similar to an error function profile) over a length about $l_d = 100$ μm,[25] a length much lower than the one of the cavity. Finally, the temperature is only affected laterally up to a distance of the order of l_d around the resistors, thus opening the way to use several independent actuators on the same system. Finally, two couples of fluids have been studied, considering that the continuous phase is always composed of deionized water with SDS, the dispersed phase is either air (bubble) or fluorinated oil (droplet). The system is exposed to an oxygen plasma and is thus hydrophilic. This property leads to the presence of a wetting film between the element and the walls.

Experimental temperature profile

The linearity of the temperature profile associated with the geometry yielded by the optimization routine could be validated experimentally. To carry this step out, we utilized a heat-sensitive fluorophore, *i.e.* rhodamine B.[27,28] By filling the cavity with a solution containing this fluorophore and then comparing the intensity of fluorescence on both series of the images acquired before and after heating, the temperature distribution can be easily measured.[21] Temperature as a function of the subsequent position has been depicted in Fig. 3a, which indicates that the temperature distribution associated with heating resistor follows a linear profile. Using the same method, we also verified that the temperature gradient varies linearly with the heating power, with a gain about 20 K mm^{-1} W^{-1} (Fig. 3b).

One key factor for ensuring success when implementing this type of actuation is the transient heat state duration, which directly affects transition time from one state to the next. Fig. 4 presents the average non-dimensional gradient variation over time. It should be pointed out that a temperature value equal to 90% of the ultimate value is reached after around 0.7 s.

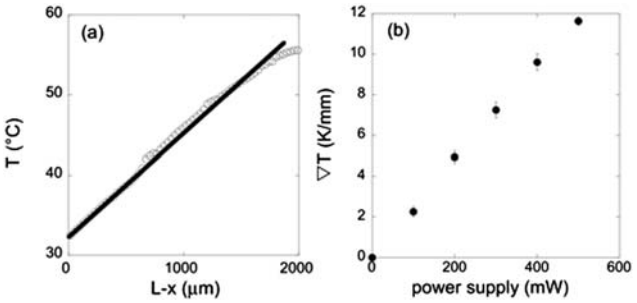

Fig. 3 (a) Experimental evolution of temperature *vs.* position inside the cavity for a heating power of 0.5 W. L is the cavity size in the x direction; (b) Evolution of average gradient *vs.* heating power.

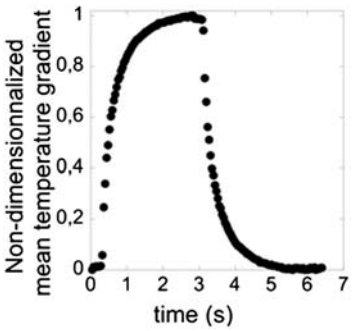

Fig. 4 Time evolution of the non-dimensional mean temperature gradient (with respect to the maximum temperature gradient) within the cavity over time.

Once the root of the system is settled, the space within the cavity then provides the setting for the three applications that are detailed below.

Applications

Displacing application

In the section "Principle" it is shown that the actuation is able to displace elements along the cavity and Fig. 1 shows the element velocity, rescaled by the surface tension gradient, as a function of both element radius and cavity thickness. Fig. 5 sketches the microfluidic cavity placed above the resistor. Fig. 6 is a stack of images showing the displacement of an element submitted to

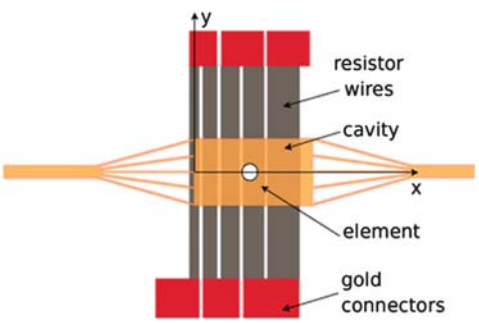

Fig. 5 Sketch of the device with the chromium resistor wires connected and placed below the microfluidic cavity.

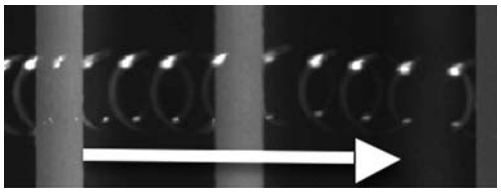

Fig. 6 Stack of images (superposition frequency is 6.66 Hz) showing an element 130 μm diameter travelling into the cavity for a temperature gradient about 4.4 K/mm.

a temperature gradient while the surrounding liquid is at rest far from the element.

It is further measured that a constant temperature gradient leads to a constant element velocity with a standard deviation below 10% along a trajectory of the order of 1 mm.

Switching application

Fig. 7 is a sketch representing the proposed switching device. It is composed of the root system and a microfluidic system containing: a T-junction device generating the elements, the actuation cavity and finally an outlet reservoir. The outlet is positioned as depicted in Fig. 7 and corresponds to a flow ratio (right channel over left channel) in the vicinity of 0.75 determined by a finite element computation (without element nor temperature gradient). The sensitivity of the outlet position on the flow rate ratio is shown in Fig. 8. Because the chosen ratio is smaller than 1 the element flows preferably towards the left channel (lower hydrodynamic resistance). In Fig. 9, it is shown that bubbles naturally flow toward the left outlet channel when the power supply is OFF; while bubbles flow towards the right outlet channel as actuation is ON. The transient stage OFF/ON and ON/OFF lasts about 250 ms.

For the three flow rates considered herein, Fig. 10a, b, c display the ratio, r, of number of bubbles flowing in the right channel to the total number of bubbles transiting in the cavity as a function of bubble emission frequency f. This quantification enables evaluating the switching efficiency. When the ratio $r = 1$, all elements are switched towards the right (Fig. 9 right); whereas when $r = 0$, all bubbles are being switched to the left (Fig. 9 left).

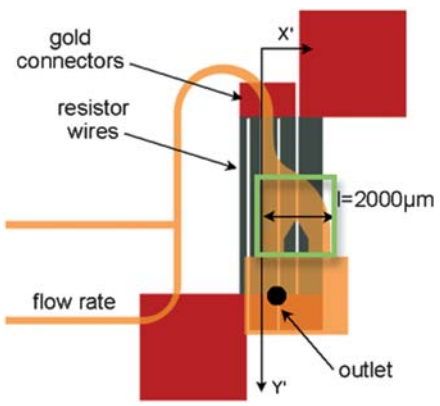

Fig. 7 Diagram of the fluidic part of the switching device, along with the heating resistance. The green square encloses what is denoted by the switching device (or actuation cavity).

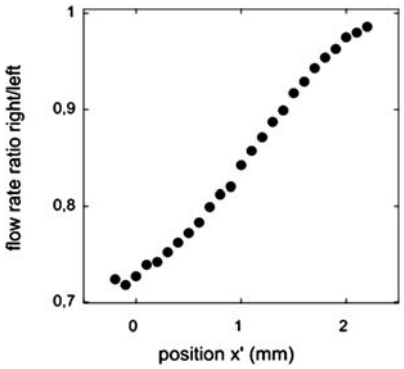

Fig. 8 Ratio of the flow rates in the two branches as a function of the outlet position. This result has been computed using finite elements (COMSOL).

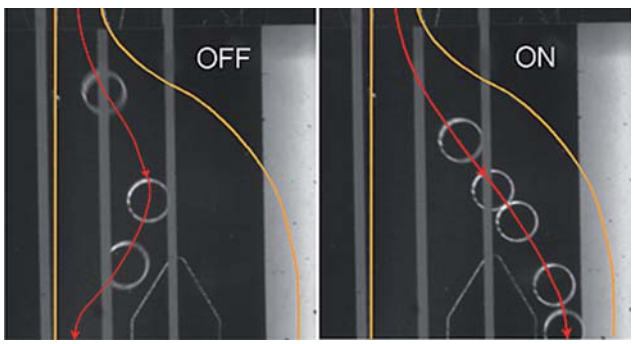

Fig. 9 Images of 300 μm diameter bubbles inside the switching device: (left) without actuation, and (right) with a 4 K/mm temperature gradient.

The cavity volume V_s (as defined in Fig. 7) is equal to 0.1 μL. The residence time for a bubble into the switching device is given by $\tau = V_s/Q$, *i.e.* $\tau = 1$ s for $Q = 5$ μL/min. Consequently, for a frequency below 1 Hz only a single bubble is present in the cavity. Hydrodynamic interactions between successive bubbles are thus negligible. For this regime, a perfect switching is obtained for a power as low as 0.1 W, *i.e.* all the bubbles are driven toward the right channel while power is on (Fig. 10a, b, c) and all bubbles are driven to the left while the power is OFF (Fig. 10d).

For higher frequencies, the number of bubbles transiting into the switching device is roughly given by $n = fV_s/Q$. The presence of a bubble into a channel modifies the hydrodynamic resistance and thus also the flow ratio. As a bubble spontaneously flows toward the lowest resistive channel, the switching efficacy can be spoiled by the presence of bubble(s) in the channels. This effect is emphasized in Fig. 10d (power OFF) which shows that above a critical frequency f_c bubbles go alternatively in both channels. Similarly, a critical frequency is also measured while power is ON. From Fig. 10a, b, c, at highest tested power supply, these critical frequencies are successively $fc = 3$ Hz for $Q = 5$ μl/min, $fc = 5$ Hz for $Q = 10$ μl/min, and $fc = 9$ Hz for $Q = 15$ μl/min. They are in agreement with the expected scaling $f_c = n_c Q/V_s$, where n_c is the critical number of bubbles in the cavity which is experimentally observed to be about 4 (whatever the flow rate).

Fig. 11 shows the switching efficiency in the case of fluorinated oil droplets into a water solution of SDS at 5 c.m.c. As for the bubble case, the switching efficiency increases while increasing the

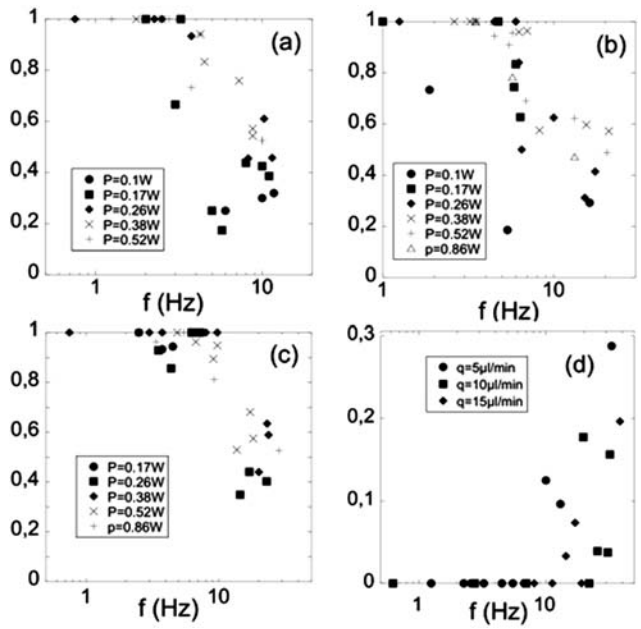

Fig. 10 Ratio *r* of the number of bubbles passing *via* the right-hand channel to the total number of bubbles transiting within the cavity for various power levels: (a) for a liquid phase flow rate of 5 µl/min; (b) for a flow rate of 10 µl/min; (c) a flow rate of 15 µl/min; and (d) ratio *r* for zero heating power and flow rates of 5 µl/min, 10 µl/min and 15 µl/min (all results have been obtained for bubbles 300 µm in diameter).

heating power. The maximal efficiency is obtained at the same order of magnitude of frequency as in the case of the bubble.

Finally actuation is found robust for both bubbles and droplets in the explored range of flow rates (from 5 µL/min up to 15 µL/min, corresponding to a velocity of the continuous phase about 1 cm/s). The main limiting factor seems to be the number of bubbles present at the same time in the switching device, *i.e.* the transiting bubble frequency.

Bubble/droplet trap

In this last application we propose a system able to trap elements, which may have a lot of practical interest in the context of applications in microfluidics or functional lab-on-a-chip. Most of the reported element trappers are based on geometry, *i.e.* elements are trapped passively;[29,30] while in the following we detail a system able to trap the elements on demand.

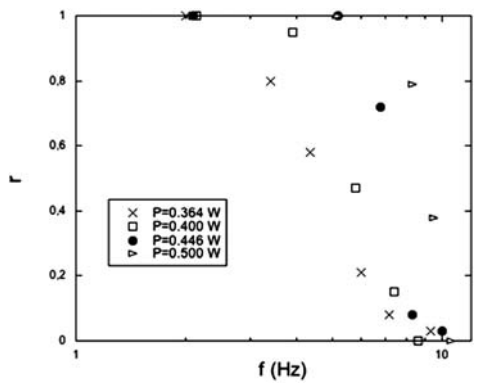

Fig. 11 Ratio *r* of the number of fluorinated droplets into water (SDS at 5 c.m.c.) passing *via* the right-hand channel to the total number of bubbles transiting within the cavity for various power levels. Typical droplet diameter is 200 µm.

Fig. 12 depicts the alveolus structure in which elements are trapped. The alveolus structure is composed of circular arcs of 140° angle, 300 µm diameter. While the temperature gradient is switched on, elements are driven and trapped into the structure even if the continuous phase is still flowing.

In Fig. 13 a stack of pictures presents the elements displacement with and without applying a temperature gradient. In this experiment, elements are bubbles in deionized water and SDS at 1.2 c.m.c. It is noticeable that the temperature gradient is sufficient to trap the elements in the alveolus structure. This trapping is obtained continuously for a power supply of 0.5 W corresponding to a temperature gradient of 11 K/mm, *i.e.* a gap of 6.6 K at the cavity scale and 3 K at the element scale. While the temperature gradient is switched off, the flow of the continuous phase is sufficient to uncouple the elements from the alveolus structure and the flow drives the elements toward the outlet. A succession temperature switch ON/OFF thus leads to a succession of elements trapping/uncoupling. The nominal range of working presented in this application is successful for elements from 180 µm to 300 µm diameter in a cavity 22 µm thick with a bubble frequency of 10 Hz and a continuous phase flow rate up to 1 µL/min.

Conclusion

From a technological point of view, this method contains many advantages in the actuation context for digital microfluidic applications, specifically a high integration rate since heating is

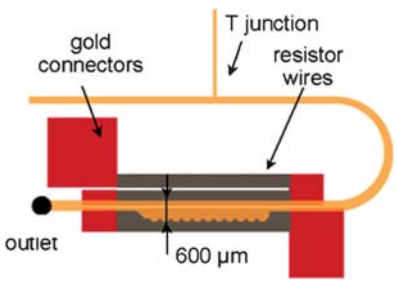

Fig. 12 Diagram of the fluidic part of the capture device, along with the heating resistance.

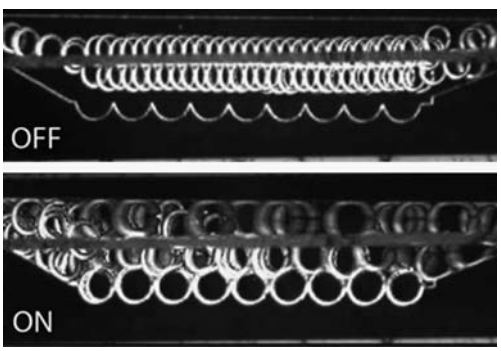

Fig. 13 Images are stacked in the two configurations: OFF/ON for a power of 0.5 W, a flow rate of 1 µL/min and a bubble frequency of about 10 Hz.

performed *in situ* within the microsystem (no need for an external device). Furthermore, the device supply does not require any specific energy quality (*i.e.* no particularly high electric voltage, U about 10 V) or high power rating (0.5 W). This method thus provides a tool in the scope of transportable systems. This type of actuation is characterized by a low cost to manufacture, a simple control, no moving parts and no need for reliance upon hybrid technology (like piezoelectric elements), given that the resistance had been created by simple deposition and etching of metals (chromium and gold) with the wafer substrate.

Another key point is that this method allows an important confinement, compatible with miniaturization, since the element velocity increases while the cavity thickness decreases. Indeed, the model predicts an element velocity inversely proportional to the cavity thickness (cavity thickness), see eqn (1).

In addition, this technique is robust whatever the surfactant used or the interface (liquid/liquid or gas/liquid). Furthermore, this method does not require the addition of a fluorophore in the liquid phase like for the methods using Marangoni stresses induced by a laser[10,31] which is a limitation in the context of biological or chemical application.

Otherwise, system thermal pollution is limited since just the zone of interest is being heated and the temperature rise remains small (only 9 K along the whole cavity of 2.5 mm for a power of 0.2 W for the switching device and only 3 K along the element for the trapper).

Finally, manufacturing and use are comfortable as shown through the three applications. This paper aims at showing the large potential of such a system and we think geometrical and dynamical parameters of devices could be adjusted in accordance with the aimed application: designing and dimensioning a system can be provided using the model presented in ref. 22.

Acknowledgements

The authors are grateful to Fabrice Monti for technical help and Patrick Tabeling for their hospitality at the MMN laboratory. The authors wish to thank CNRS, ESPCI and Rennes Métropole for financial support. Isabelle Cantat is supported by Institut Universitaire de France.

References

1 B. Zheng and R. F. Ismagilov, A microfluidic approach for screening submicroliter volumes against multiple reagents by using preformed arrays of nanoliter plugs in a three-phase liquid/liquid/gas flow., *Angew. Chem., Int. Ed.*, 2005, **44**, 2520–2523.
2 H. Song and R. F. Ismagilov, Millisecond kinetics on a microfluidic chip in multiphase microfluidics at low values of the Reynolds and capillary numbers, *J. Am. Chem. Soc.*, 2003, **125**, 14613.
3 K. Jensen and A. Lee, The science and applications of droplets in microfluidics devices, *Lab Chip*, 2004, **4**, 31N–32N.
4 H. Song, D. L. Chen and R. F. Ismagilov, Reactions in Droplets in Microfluidic Channels, *Angew. Chem., Int. Ed.*, 2006, **45**(44), 7336–7356.
5 P. S. Dittrich and P. Schwille, An Integrated Microfluidic System for Reaction, High-Sensitivity Detection, and Sorting of Fluorescent Cells and Particles, *Anal. Chem.*, 2003, **75**(21), 5767–5774.
6 T. P. Hunt, H. Lee and R. M. Westervelt, Addressable micropost array for the dielectrophoretic manipulation of particles in fluid, *Appl. Phys. Lett.*, 2004, **85**(26), 6421.
7 K. Ahn, C. Kerbage, T. P. Hunt and R. M. Westervelt, Dielectrophoretic manipulation of drops for high-speed microfluidic sorting devices, *Appl. Phys. Lett.*, 2006, **88**(2), 024104.
8 A. Y. Fu, H. P. Chou, C. Spence, F. H. Arnold and S. R. Quake, An integrated microfabricated cell sorter, *Anal. Chem.*, 2002, **74**, 2451.
9 Z. Jiao, N.-T. Nguyen and X. Huang, Reciprocating thermocapillary plug motion in an externally heated capillary, *AIChE*, 2007, **45**(2), 350–366.
10 N.-T. Nguyen and X. Huang, Thermocapillary effect of a liquid plug in transient temperature fields, *Jpn. J. Appl. Phys.*, 2005, **44**, 1139–1142.
11 A. A. Darhuber, J. P. Valentino, J. M. Davis and S. M. Troian, Microfluidic actuation by modulation of surface stresses, *Appl. Phys. Lett.*, 2003, **82**, 657–659.
12 A. A. Darhuber, J. P. Valentino, S. M. Troian and S. Wagner, Thermocapillary actuation of droplets on chemically patterned surfaces by programmable microheater arrays, *J. Microelectromech. Syst.*, 2003, **12**, 873–879.
13 Z. Jiao, X. Huang and N.-T. Nguyen, Thermocapillary actuation of droplet in a planar microchannel, *Microfluid. Nanofluid.*, 2008, **5**, 205–214.
14 E. Lajeunesse and G. M. Homsy, Thermocapillary migration of long bubbles in polygonal tubes, *Phys. Fluids*, 2003, **15**, 308–314.
15 C. N. Baroud, J.-P. Delville, F. Gallaire and R. Wunenburger, Thermocapillary valve for droplet production and sorting, *Phys. Rev. E: Stat., Nonlinear, Soft Matter Phys.*, 2007, **75**, 046302.
16 J.-P. Delville, M. Robert de Saint Vincent, R. D. Schroll, H. Chraïbi, B. Issenmann, R. Wunenburger, D. Lasseux, W. W. Zhang and E. Brasselet, Laser microfluidics: fluid actuation by light, *J. Opt. A: Pure Appl. Opt.*, 2009, **11**, 034015.
17 T. H. Ting, Y. F. Yap, N.-T. Nguyen, T. N. Wong and J. C. K. Chai, Thermally mediated breakup of drops in microchannels, *Appl. Phys. Lett.*, 2006, **89**, 234101.
18 Y.-F. Yap, S.-H. Tan, N.-T. Nguyen, S. M. Sohel Murshed, T.-N. Wong and L. Yobas, Thermally mediated control of liquid microdroplets at a bifurcation, *J. Phys. D: Appl. Phys.*, 2009, **42**, 065503.
19 M.-C. Jullien, M.-J. Tsang Mui Ching, C. Cohen, L. Ménétrier and P. Tabeling, Droplet breakup in microfluidic T-junctions at small capillary numbers, *Phys. Fluids*, 2009, **21**, 072001.
20 T. Squires and S. Quake, Microfluidics: fluid physics at the nanoliter scale, *Rev. Mod.Phys.*, 2005, **77**, 977–1026.
21 B. Selva, J. Marchalot and M.-C. Jullien, An optimized resistor pattern for temperature gradient control in microfluidics, *J. Micromech. Microeng.*, 2009, **19**, 065002.
22 B. Selva, I. Cantat and M.-C. Jullien, Migration of a bubble towards higher surface tension under the effect of thermocapillary stress, *preprint*, 2009.
23 E. Terriac, F. Artzner, A. Moreac, C. Meriadec, P. Chaslep, J.-C. Ameline, J. Ohana and J. Emile, Structure of liquid films of an ordered foam confined in a narrow channel, *Langmuir*, 2007, **23**, 12055–12060.
24 E. Guyon, J. -P. Hulin, L. Petit, Hydrodynamique physique, CNRS editions - EDP Sciences, 2001.
25 B. Selva, P. Mary and M.-C. Jullien, Integration of a uniform and rapide heating source into microfluidic systems, *Microfluid. Nanofluid.*, 2009, DOI: 10.1007/s10404-009-0505-7; Y. Xia and G. M. Whitesides, Soft lithography, *Annu. Rev. Mater. Sci.*, 1998, **28**, 153–184.
26 K. Deb, A. Pratap, S. Agarwal and T. Meyarivan, A fast and elitist multiobjective genetic algorithm: NSGA-II, *IEEE Trans. Evol. Comput.*, 2002, **6**(2), 182–197.
27 D. Ross, M. Gaitan and L. E. Locascio, Temperature measurement in microfluidic systems using a temperature-dependent fluorescent dye, *Anal. Chem.*, 2001, **73**(17), 4117–4123.
28 D. Erickson, D. Sinton and D. Li, Joule heating and heat transfer in poly (dimethylsiloxane) microfluidic systems, *Lab Chip*, 2003, **3**, 141–149.
29 H. Boukellal, S. Selimovi, Y. J. Galder Cristobal and S. Fraden, Simple, robust storage of drops and fluids in a microfluidic device, *Lab Chip*, 2009, **9**, 331–338.
30 N. R. Beer, K. A. Rose and I. M. Kennedy, Monodisperse droplet generation and rapid trapping for single molecule detection and reaction kinetics measurement, *Lab Chip*, 2009, **9**, 841–844.
31 A. T. Ohta, A. Jamshidi, J. K. Valley, H.-Y. Hsu and M. C. Wu, Optically actuated thermocapillary movement of gas bubbles on an absorbing substrate, *Appl. Phys. Lett.*, 2007, **91**, 074103.

